

Exploring glueball wave functions on the lattice

Rajan Gupta

*Institute for Theoretical Physics, University of California, Santa Barbara, California 93106
and T-8, MS-B285, Los Alamos National Laboratory, Los Alamos, New Mexico 87545*

Apoorva Patel

*Institute for Theoretical Physics, University of California, Santa Barbara, California 93106
and Supercomputer Education and Research Centre and Centre for Theoretical Studies,
Indian Institute of Science, Bangalore 560012, India*

Clive F. Baillie

*Physics Department, University of Boulder, Boulder, Colorado 80309
and Physics Department, Caltech, Pasadena, California 91125*

Gregory W. Kilcup

*Institute for Theoretical Physics, University of California, Santa Barbara, California 93106
and Physics Department, Ohio State University, Columbus, Ohio 43210*

Stephen R. Sharpe

*Institute for Theoretical Physics, University of California, Santa Barbara, California 93106
and Physics Department, University of Washington, Seattle, Washington 98195*

(Received 13 December 1990)

We calculate the string tension and 0^{++} and 2^{++} glueball masses in pure gauge QCD using an improved lattice action. We compare various smearing methods, and find that the best glueball signal is obtained using smeared Wilson loops of a size of about 0.5 fm. Our results for mass ratios $m_{0^{++}}/\sqrt{\sigma}=3.5(3)$ and $m_{2^{++}}/m_{0^{++}}=1.6(2)$ are consistent with those computed with the simple plaquette action.

I. INTRODUCTION

Numerical lattice calculations provide strong evidence for the existence of a mass gap in pure gauge QCD.¹ Though straightforward in principle, these calculations are hampered by large statistical errors, with the problems becoming more severe as the continuum limit is approached.² In this paper we investigate methods to improve the signal, and give new results for the scalar and tensor glueball masses in pure gauge QCD.

Although the spectrum of pure gauge QCD cannot be directly compared to experiment, it is important to pin it down because we know so little about glueball properties. The guidance from theoretical calculations in various models is only qualitative. For example, models agree that the lightest glueball is a scalar, but differ substantially on its mass.³ Definite numbers for pure gauge QCD would give a solid base from which to attempt phenomenological studies. Furthermore, it is important to study methods for improving the signal, for they will be directly applicable to future calculations in full QCD.

The major progress in the last few years has come from improving the operators used to couple to the glueballs. The main innovation has been the use of smeared operators. This increases the overlap with the lowest state and reduces contamination from higher states, resulting in correlators which reach their asymptotic behavior at

smaller time separations. In addition, the noise from ultraviolet fluctuations is reduced.

The two popular smearing methods are those proposed by Teper⁴ and DeGrand,⁵ and by the APE Collaboration.⁶ The quality of the signal in two-point functions using these operators is significantly improved compared to unsmeared operators. In this paper we propose an alternative way of constructing glueball operators using a slight variation of the APE smearing method, and find that our variant improves the signal for a fixed number of smearing steps. We also subject the source method to a critical analysis and make a detailed comparison of the methods of Teper and DeGrand and APE. Finally we present results for the string tension σ and the glueball masses $m_{0^{++}}$ and $m_{2^{++}}$ from our runs with the largest statistics. Our statistics are comparable to those of the best previous calculations,^{7,8} and our results are in agreement.

We use an improved gauge action consisting of four terms: the plaquette in the fundamental (3), adjoint (8) and 6 representations, and the 1×2 loop in the fundamental representation. The couplings are taken in the proportion

$$\frac{K_8}{K_F} = -0.12, \quad \frac{K_6}{K_F} = -0.12, \quad \frac{K_{1 \times 2}}{K_F} = -0.04, \quad (1.1)$$

with the traces normalized to unity. All results reported here are with $K_F=10.5$. By matching the string tension, we estimate that this corresponds to $K_F \approx 5.96$ for the Wilson action ($K_8=K_6=K_{1 \times 2}=0$). Our improved action was determined by a Monte Carlo renormalization-group (MCRG) calculation to lie close to the renormalized trajectory for the $\sqrt{3}$ renormalization group transformation.⁹ The main advantage of this action over the simple plaquette action is that it lies farther from the line of phase transitions in the fundamental-adjoint coupling plane. Although this line of phase transitions is a lattice artifact, it does lower the 0^{++} glueball mass for Wilson action with $K_F < 6.0$. In a previous paper,¹⁰ we calculated σ and $m_{0^{++}}$, at $K_F=9.9$ and 10.5 , using a cold wall source, and on fairly small lattices.

II. CALCULATIONAL DETAILS

Details of our data samples are given in Table I. The lattice update is done using a combination of overrelaxed and Metropolis methods.¹¹ For $12^3 \times 24$ and $15^3 \times 24$ lattices every link update consists of an overrelaxed step followed by a Metropolis hit. For $9^3 \times 24$ lattices the update consists of four overrelaxed sweeps followed by one Metropolis sweep. In most cases we perform measurements every five sweeps and divide the data into bins of 400–500 measurements to do the statistical analysis. We typically have runs of 20–60 bins, and the final errors are obtained using the single-elimination jackknife method with each bin regarded as an independent data point.

We calculate masses of glueballs in the A_1^{++} and E^{++} (2-dimensional) representations of the cubic group. The former couples to the scalar glueball, the latter to the tensor. For a given size of the loop, we construct these operators by adding the various loop orientations in the standard way.¹² We do not calculate the mass for the T_2^{++} (3-dimensional) representation which along with E^{++} makes up the continuum 2^{++} representation. The string tension is calculated from correlations of spatial Polyakov lines.

The signal in the connected 2-point correlators $\Gamma(t)$ for all three observables does not last long enough to make fits to an exponential falloff. The data is therefore presented in terms of the effective mass defined as

$$m_{\text{eff}}(t) = \ln \frac{\Gamma(t-1)}{\Gamma(t)}. \quad (2.1)$$

In the case of A_1^{++} , the connected correlator may contain a sizable constant term on a finite lattice. This is because the glueball can propagate around the lattice, with the operators acting as scalar insertions. In such cases, to ensure the validity of our results, we make checks using

$$m'_{\text{eff}}(t) = \frac{\Gamma(t-1) - \Gamma(t)}{\Gamma(t) - \Gamma(t+1)}. \quad (2.2)$$

III. SMEARING METHODS

The operators commonly used for measuring glueball masses are Wilson loops. The simplest choice—the plaquette, 1×2 loop, etc.—suffer from two problems. First, they are much smaller than the glueballs, so that the signal in the correlators is weak. Second, they couple strongly to ultraviolet fluctuations, increasing the noise in the correlators. For a fixed loop size, both problems get worse as the lattice spacing is decreased. For a detailed discussion see Ref. 2. To resolve these problems one needs to construct operators that are “fat.” This both increases the overlap with the lowest-lying states, and decreases the ultraviolet fluctuations. All the methods discussed below have the following common features.

(a) Loops are made fat by using smeared links. The smearing is done by averaging the gauge field associated with a link over its local environment. A straight path on the original lattice is replaced by a sum of paths with the same starting and ending points. This sum has the same gauge transformation property as the original “link,” so that operators constructed from closed Wilson loops made up of these smeared links are gauge invariant.

(b) The averaged link Σ , a sum of SU(3) matrices, is not an element of SU(3). The glueball operators (Wilson

TABLE I. Description of data samples on the various lattices.

Lattice	$9^3 \times 24$	$12^3 \times 24$	$12^3 \times 24$	$12^3 \times 24$	$15^3 \times 24$
Source	None	Cold wall	None	None	None
Smearing	$b=1$	$b=2$	$b=2$	$b=1$	$b=1$
Maximum N_s	6	2	2	6	6
ϵ Values	1.0	0.5, 1.0, 2.0	0.8, 1.0, 1.2	1.0, 1.25	0.25, 0.5, 0.75
Measured loops	1×1 to 4×4 Squares	$1 \times 1, 1 \times 2$ $2 \times 1, 2 \times 2$	$1 \times 1, 1 \times 2$ $2 \times 1, 2 \times 2$	1×1 to 6×6 Squares	1×1 to 6×6 Squares
Measurement interval	5 sweeps	2 sweeps	2 sweeps	5 sweeps	5 sweeps
Bin size	500	400	400	500	500
Bins for $\epsilon=1$	23	20	60	43 ($N_s=3, 4$) 20 ($N_s=5, 6$)	30
Sweeps for $\epsilon=1$	57 500	16 000	48 000	107 500	75 000

loops) can be constructed from these general 3×3 complex matrices. It is common, however, to project the sum back to $SU(3)$, as part of the definition of smearing. We perform this projection by determining the $SU(3)$ matrix V which maximizes $\text{Re Tr}(V^\dagger \Sigma)$.

(c) The smearing process is iterated N_s times to define increasingly obese links. In our notation $N_s=0$ refers to the original unsmeared lattice.

(d) Only spatial links participate in the averaging. Thus the transfer matrix for the smeared operators remains unaffected and is positive definite.

(e) One can construct operators of any size and shape using these smeared links to study different spin-parity states.

Teper and DeGrand use the scale factor 2 blocking introduced by Swendsen for MCRG studies¹³ as the template for smearing. The construction of the fat link is shown in Fig. 1. The smearing reduces the number of points in a time slice by the factor 2^3 , so for a given size lattice the smearing operation can be repeated only a limited number of times. This is a quick and easy procedure for making the link “fat” and for getting large loops because a loop of side L on level N_s corresponds to size $L \times 2^{N_s}$ on the original lattice. Michael and Teper⁸ find that their best results come from $N_s=2$, i.e., large fat loops have the best overlap with glueballs. In our runs using this method, we average over all the 2^3 blocking constructions at each level in order to improve the statistics. We refer to this method as $b=2$ smearing.

The method proposed by the APE Collaboration is illustrated in Fig. 2. Each link on the lattice is replaced by the average of itself and the sum of the four staples in the two spatial dimensions transverse to the link direction. The staples are added with weight ϵ . In contrast with the method of Teper and DeGrand, each individual link is smeared, so that the number of points on a time slice remains constant. The lattice made up of these fat links is operationally identical to the original lattice. The smearing process is easily iterated, using these fat links to construct the next level of fat links, etc.

In actual applications the APE group began with the plaquette, and smeared repeatedly using a small value of the smearing parameter, $\epsilon=0.2$. This smearing builds up a fat link with an approximate $\exp(-\tau \mathbf{k}_\perp^2)$ behavior in momentum space, with the length scale in lattice units given by $\tau=N_s \epsilon$.⁶ With positive-definite correlators, one expects that at a fixed t the mass estimate m_{eff} would first improve with N_s , as the overlap with the lightest glueball state improves. For N_s too large, however, the scale exceeds the size of the ground-state glueball and m_{eff} should increase. This is indeed what the APE group

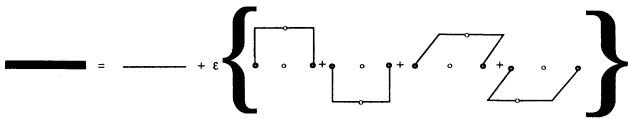


FIG. 1. $b=2$ smearing for construction of fat links.

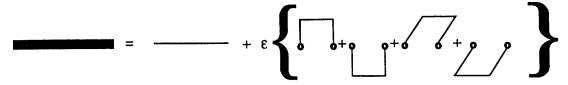


FIG. 2. $b=1$ smearing for construction of fat links.

finds:¹⁴ for $\epsilon=0.2$ there is a minimum in the 0^{++} mass at $N_s \approx 25$.

The method we use is an extension of the APE method, differing in two ways. First, we apply the smearing to loops of varying sizes. In the present study we use square loops of size up to 6×6 . Given that studies of $b=2$ smearing find large loops give better signals, it is reasonable to expect that the same will apply to APE smearing. This is particularly true for nonzero spin representations, for which one has to take the difference of smeared loops oriented in different directions. If the starting loop is too small, then, after many smearing steps, the resulting sum of tangled loops will be almost spherical, and there will be a large cancellation when one takes differences.

The second change in the method is that we extend the calculation to larger values of ϵ , using a range of values between 0.25 and 1.50. For $\epsilon \approx 1$, the calculation is similar to a blocking transformation. Compared to smearing with small ϵ , the resulting sum of loops has a sharper profile and the smearing fattens the loops much more quickly.

We refer to this method as $b=1$ smearing. Whether or not these extensions of the APE method improve the signal can only be decided by numerical tests. Our comparative study described in the following sections finds that, for $a^{-1} \approx 2$ GeV, the best glueball signal is obtained using 5×5 loops and $\epsilon \approx 1, N_s \approx 5$.

IV. TUNING THE SMEARING PARAMETERS

There are three parameters to be tuned when using the smearing methods: the smearing weight ϵ ; the number of times that smearing is repeated, N_s ; and the size and shape of the Wilson loop operators. We optimize these parameters by studying the effective mass deduced from $t=0/1$ and $1/2$. We search for the operator that gives the smallest m_{eff} , for this has the largest overlap with the lightest state and less contamination from the heavier states. This amounts to a discrete search among variational wave functions. In addition, among the operators with small m_{eff} , we prefer those with the smallest error in m_{eff} . In general the optimum choices depend on the quantity being calculated; in fact we find optimal parameters for the string tension and glueball masses to be similar.

As indicated in Table I, our most extensive tests are for $b=1$ smearing on the $15^3 \times 24$ lattices. The results for σL , $m_{0^{++}}$, and $m_{2^{++}}$ are collected in Tables II(a), II(b), and II(c), respectively. Table II(a) shows that the operator overlap improves significantly as N_s increases. Looking at the $t=0/1$ data, we see that for each fixed N_s there appears to be an optimal ϵ . As N_s increases, the optimal ϵ decreases; for $N_s=6$ it is about $\epsilon=1$. The resulting

TABLE II. (a) Comparison of the string tension as a function of the smearing weight ϵ and the smearing level N_s on $15^3 \times 24$ lattices. Weights $\epsilon=0.25, 0.50, 0.75, 1.5$ data use the same 6000 configurations. The $\epsilon=1.25$ data uses only the last 3500 of these configurations. Our estimate is $\sigma L=0.72(4)$ from time separation 3–5 using the $\epsilon=1.0$ large statistics (15 000 configurations) data. (b) Comparison of the 0^{++} glueball mass for the same runs as in (a). The data is for time separation 0–1. Our best estimate is $m_{0^{++}}=0.78(4)$ from time separation 2–4. (c) Comparison of the 2^{++} glueball mass for the same runs as in (a). The data is for time separation 0–1. Our best estimate is $m_{2^{++}}=1.19(5)$ from time separation 2–4.

(a)						
σL from time separation 0–1						
N_s	$\epsilon=0.25$	$\epsilon=0.50$	$\epsilon=0.75$	$\epsilon=1.0$	$\epsilon=1.25$	$\epsilon=1.5$
3	1.523(10)	1.332(09)	1.266(09)	1.233(06)	1.216(08)	1.200(09)
4	1.343(10)	1.190(09)	1.137(09)	1.109(06)	1.098(08)	1.088(09)
5	1.226(09)	1.097(09)	1.052(09)	1.029(06)	1.025(09)	1.026(10)
6	1.143(09)	1.030(09)	0.991(09)	0.975(06)	0.990(10)	1.035(11)
σL from time separation 1–2						
N_s	$\epsilon=0.25$	$\epsilon=0.50$	$\epsilon=0.75$	$\epsilon=1.0$	$\epsilon=1.25$	$\epsilon=1.5$
3	1.097(31)	1.047(26)	1.024(25)	1.016(14)	0.990(23)	0.995(24)
4	1.051(27)	1.000(24)	0.979(24)	0.971(13)	0.950(24)	0.950(23)
5	1.014(25)	0.965(23)	0.945(23)	0.939(13)	0.921(25)	0.916(23)
6	0.985(24)	0.938(22)	0.919(22)	0.913(13)	0.897(27)	0.887(24)
(b)						
$m_{0^{++}}$ from 1×1 loop						
N_s	$\epsilon=0.25$	$\epsilon=0.50$	$\epsilon=0.75$	$\epsilon=1.0$	$\epsilon=1.25$	$\epsilon=1.5$
3	1.57(1)	1.51(3)	3.0(1)	3.9(1)		
4	1.42(1)	1.38(1)	3.8(1)	4.7(2)		
5	1.26(2)	1.35(1)	4.8(3)	5.1(3)		
6	1.18(1)	1.12(3)	6.0(8)	5.2(3)		
$m_{0^{++}}$ from 2×2 loop						
N_s	$\epsilon=0.25$	$\epsilon=0.50$	$\epsilon=0.75$	$\epsilon=1.0$	$\epsilon=1.25$	$\epsilon=1.5$
3	1.40(1)	1.29(1)	1.24(1)	1.21(1)	1.20(1)	1.22(1)
4	1.29(1)	1.18(1)	1.14(1)	1.10(1)	1.12(1)	1.16(1)
5	1.21(1)	1.10(1)	1.06(1)	1.03(1)	1.10(1)	1.34(1)
6	1.14(1)	1.04(1)	1.00(1)	0.99(1)	1.33(1)	2.79(4)
$m_{0^{++}}$ from 3×3 loop						
N_s	$\epsilon=0.25$	$\epsilon=0.50$	$\epsilon=0.75$	$\epsilon=1.0$	$\epsilon=1.25$	$\epsilon=1.5$
3	1.24(1)	1.16(1)	1.13(1)	1.10(1)	1.10(1)	1.11(1)
4	1.16(1)	1.08(1)	1.05(1)	1.03(1)	1.06(1)	1.11(1)
5	1.10(1)	1.02(1)	1.00(1)	1.00(1)	1.15(1)	1.52(1)
6	1.05(1)	0.98(1)	0.96(1)	1.05(1)	1.80(1)	3.28(8)
$m_{0^{++}}$ from 4×4 loop						
N_s	$\epsilon=0.25$	$\epsilon=0.50$	$\epsilon=0.75$	$\epsilon=1.0$	$\epsilon=1.25$	$\epsilon=1.5$
3	1.14(1)	1.06(1)	1.04(1)	1.01(1)	1.01(1)	1.01(1)
4	1.07(1)	1.00(1)	0.98(1)	0.95(1)	0.96(1)	0.96(1)
5	1.01(1)	0.95(1)	0.93(1)	0.91(1)	0.93(1)	0.96(1)
6	0.98(1)	0.92(1)	0.90(1)	0.88(1)	0.94(1)	1.27(1)
$m_{0^{++}}$ from 5×5 loop						
N_s	$\epsilon=0.25$	$\epsilon=0.50$	$\epsilon=0.75$	$\epsilon=1.0$	$\epsilon=1.25$	$\epsilon=1.5$
3	1.18(2)	1.07(1)	1.03(1)	1.00(1)	1.00(1)	0.99(1)
4	1.07(1)	0.98(1)	0.95(1)	0.93(1)	0.93(1)	0.93(1)
5	1.00(1)	0.93(1)	0.90(1)	0.89(1)	0.90(1)	0.91(1)
6	0.95(1)	0.89(1)	0.87(1)	0.86(1)	0.90(1)	1.07(1)

TABLE II. (Continued).

(b)						
$m_{0^{++}}$ from 6×6 loop						
N_s	$\epsilon=0.25$	$\epsilon=0.50$	$\epsilon=0.75$	$\epsilon=1.0$	$\epsilon=1.25$	$\epsilon=1.5$
3	1.45(2)	1.24(2)	1.17(2)	1.14(1)	1.12(2)	1.10(2)
4	1.25(2)	1.09(2)	1.04(2)	1.01(1)	1.01(2)	0.99(2)
5	1.12(2)	1.00(2)	0.96(2)	0.94(1)	0.94(2)	0.95(2)
6	1.04(2)	0.94(2)	0.91(2)	0.90(1)	0.92(2)	1.01(1)
(c)						
$m_{2^{++}}$ from 1×1 loop						
N_s	$\epsilon=0.25$	$\epsilon=0.50$	$\epsilon=0.75$	$\epsilon=1.0$	$\epsilon=1.25$	$\epsilon=1.5$
3	2.06(2)	2.04(2)	3.8(1)	5.2(2)		
4	1.88(2)	1.83(1)	4.3(1)	5.7(3)		
5	1.78(1)	1.74(1)	4.7(2)	5.8(4)		
6	1.68(4)	1.79(5)	5.0(2)	5.8(4)		
$m_{2^{++}}$ from 2×2 loop						
N_s	$\epsilon=0.25$	$\epsilon=0.50$	$\epsilon=0.75$	$\epsilon=1.0$	$\epsilon=1.25$	$\epsilon=1.5$
3	1.85(1)	1.71(1)	1.66(1)	1.64(1)	1.64(1)	1.66(1)
4	1.72(1)	1.59(1)	1.55(1)	1.53(1)	1.55(1)	1.63(1)
5	1.63(1)	1.50(1)	1.46(1)	1.46(1)	1.55(1)	1.81(1)
6	1.55(1)	1.44(1)	1.40(1)	1.43(1)	1.72(1)	2.53(2)
$m_{2^{++}}$ from 3×3 loop						
N_s	$\epsilon=0.25$	$\epsilon=0.50$	$\epsilon=0.75$	$\epsilon=1.0$	$\epsilon=1.25$	$\epsilon=1.5$
3	1.64(1)	1.55(1)	1.52(1)	1.50(1)	1.49(1)	1.51(1)
4	1.55(1)	1.47(1)	1.44(1)	1.44(1)	1.46(1)	1.54(1)
5	1.49(1)	1.41(1)	1.38(1)	1.42(1)	1.60(1)	2.00(1)
6	1.44(1)	1.36(1)	1.34(1)	1.52(1)	2.26(3)	3.36(6)
$m_{2^{++}}$ from 4×4 loop						
N_s	$\epsilon=0.25$	$\epsilon=0.50$	$\epsilon=0.75$	$\epsilon=1.0$	$\epsilon=1.25$	$\epsilon=1.5$
3	1.51(1)	1.43(1)	1.40(1)	1.38(1)	1.37(1)	1.38(1)
4	1.43(1)	1.36(1)	1.34(1)	1.32(1)	1.32(1)	1.33(1)
5	1.38(1)	1.31(1)	1.29(1)	1.28(1)	1.29(1)	1.35(1)
6	1.34(1)	1.28(1)	1.26(1)	1.26(1)	1.33(1)	1.57(1)
$m_{2^{++}}$ from 5×5 loop						
N_s	$\epsilon=0.25$	$\epsilon=0.50$	$\epsilon=0.75$	$\epsilon=1.0$	$\epsilon=1.25$	$\epsilon=1.5$
3	1.55(1)	1.42(1)	1.38(1)	1.35(1)	1.34(1)	1.34(1)
4	1.42(1)	1.33(1)	1.30(1)	1.28(1)	1.27(1)	1.28(1)
5	1.35(1)	1.27(1)	1.25(1)	1.24(1)	1.25(1)	1.28(1)
6	1.30(1)	1.24(1)	1.22(1)	1.22(1)	1.27(1)	1.45(1)
$m_{2^{++}}$ from 6×6 loop						
N_s	$\epsilon=0.25$	$\epsilon=0.50$	$\epsilon=0.75$	$\epsilon=1.0$	$\epsilon=1.25$	$\epsilon=1.5$
3	1.80(1)	1.58(1)	1.51(1)	1.47(1)	1.45(1)	1.44(1)
4	1.59(1)	1.43(1)	1.37(1)	1.34(1)	1.33(1)	1.33(1)
5	1.46(1)	1.33(1)	1.29(1)	1.27(1)	1.27(1)	1.30(1)
6	1.38(1)	1.27(1)	1.24(1)	1.23(1)	1.27(1)	1.40(1)

operator improves as N_s increases, suggesting that the best operator will have large N_s and small ϵ , and thus be smooth like the operators used by APE.⁶ It is costly, however, to use too large an N_s , and our results show that a reasonable alternative is to use moderate N_s and a large ϵ .

Similar conclusions follow from our results for glueball masses [Tables II(b) and II(c)]. Here we can vary the

loop sizes as well, and we find that 5×5 loops are optimal, with 4×4 and 6×6 being almost indistinguishable. For these loops, and for $N_s=6$ the optimal ϵ is again close to 1. The signal in the 1×1 loop shows a very different behavior: it exists only for $\epsilon=0.25$ and 0.5, and the convergence with N_s is slow. This is consistent with the findings of APE that when using the 1×1 loop as a template, the best signal with $\epsilon=0.2$ is obtained with

TABLE III. (a) The σL data for $b=2$ smearing with $\epsilon=1.0$ on $12^3 \times 24$ lattices. The results in the last column are with a cold wall source, while the rest of the data is without any source. (b) The data for $m'_{0^{++}}$ for the same runs as in (a). (c) The data for $m_{2^{++}}$ for the same runs as in (a).

(a)				
$b=2$ smearing: σL on $12^3 \times 24$ lattices				
t	$N_s=0$	$N_s=1$	$N_s=2$	$N_s=2$
0-1	3.643(033)	1.316(007)	0.780(006)	
1-2	1.039(090)	0.848(011)	0.700(009)	0.744(004)
2-3	0.574(218)	0.676(023)	0.653(015)	0.594(007)
3-4		0.629(032)	0.642(026)	0.554(014)
4-5		0.664(073)	0.617(049)	0.571(019)
5-6		0.619(130)	0.609(089)	0.579(030)
6-7			0.516(143)	0.621(044)
7-8				0.642(082)
8-9				0.616(173)

(b)				
$b=2$ smearing: $m'_{0^{++}}$ on $12^3 \times 24$ lattices				
t	$N_s=0$	$N_s=1$	$N_s=2$	$N_s=2$
$m'_{0^{++}}$ using 1×1 loop				
0-1-2	3.03(04)	1.69(01)	0.98(01)	
1-2-3		1.44(05)	0.92(02)	1.23(01)
2-3-4		1.18(13)	0.93(05)	0.91(02)
3-4-5		1.00(41)	0.93(12)	0.68(04)
4-5-6			0.90(25)	0.73(06)
5-6-7			0.62(47)	0.73(17)
6-7-8				0.97(41)
$m'_{0^{++}}$ using 1×2 loop				
0-1-2	2.82(03)	1.55(01)	1.04(01)	
1-2-3		1.30(04)	0.90(02)	
2-3-4		1.07(11)	0.90(04)	
3-4-5		1.24(35)	0.88(11)	
4-5-6			0.84(21)	
5-6-7			0.67(46)	
$m'_{0^{++}}$ using 2×2 loop				
0-1-2	2.43(02)	1.43(01)	1.64(01)	
1-2-3	1.68(11)	1.13(03)	1.10(04)	
2-3-4		0.95(09)	1.07(10)	
3-4-5		1.21(26)	0.96(30)	

(c)			
$b=2$ smearing: $m_{2^{++}}$ on $12^3 \times 24$ lattices			
t	$N_s=0$	$N_s=1$	$N_s=2$
$m_{2^{++}}$ using 1×1 loop			
0-1	3.68(04)	2.15(01)	1.39(01)
1-2		1.88(06)	1.34(01)
2-3		1.75(30)	1.24(06)
3-4			1.44(20)
$m_{2^{++}}$ using 1×2 loop (oblate)			
0-1	3.40(02)	1.94(01)	1.38(01)
1-2	3.02(55)	1.73(03)	1.30(01)
2-3		1.46(14)	1.20(05)
3-4			1.14(13)
4-5			0.94(38)

TABLE III. (Continued).

(c)			
$b=2$ smearing: $m_{2^{++}}$ on $12^3 \times 24$ lattices			
t	$N_s=0$	$N_s=1$	$N_s=2$
$m_{2^{++}}$ using 2×1 loop (prolate)			
0-1	3.40(02)	1.94(01)	1.39(01)
1-2	3.05(57)	1.70(03)	1.29(01)
2-3		1.48(15)	1.20(06)
3-4			1.29(17)
4-5			1.55(86)
$m_{2^{++}}$ using 2×2 loop			
0-1	2.93(02)	1.74(01)	1.73(01)
1-2	2.34(19)	1.50(02)	1.39(02)
2-3		1.42(10)	1.21(07)
3-4		2.02(64)	1.38(27)

~ 25 smearing steps.¹⁴

Runs on $9^3 \times 24$ and $12^3 \times 24$ lattices yield similar conclusions, so there is little volume dependence in the tuning. Based on these results, and our choice that $N_s^{\max}=6$, we use $\epsilon=1$ for our large statistics runs. The results for $12^3 \times 24$ and $15^3 \times 24$ lattices are given in Tables IV and V, respectively.

Our tests of $b=2$ smearing have been done on $12^3 \times 24$ lattices (see Table I). Partial results are shown in Tables III(a)–III(c). Looking at the $t=0/1$ results, we see a marked improvement with increasing N_s . For $N_s=2$ (the largest possible value) we find $\epsilon \approx 1$ to be optimal.

V. COMPARISON WITH THE COLD WALL SOURCE METHOD

The source method is useful because it extends the time range of the signal. It has, however, two disadvantages. The first is the need for optimizing the source for each state of interest, e.g., the commonly used cold wall source couples strongly only to the torelon (of energy σL) and the 0^{++} glueball. (By modifying the cold wall source so

that links in only two space directions are set to identity at $t=0$, one can generate a coupling to the 2^{++} glueball as well.) The more important problem is that correlators are not positive definite; they can, and often do, approach the asymptotic result from below. On the contrary, simulations without external sources have the advantages that (a) different spin-parity states can be studied using the same set of lattice configuration, and (b) the correlators are positive definite so that mass estimates approach their asymptotic values from above. The disadvantage is that the signals are noisier.

For $b=2$ smearing, we have compared the signals obtained with and without a cold wall source on $12^3 \times 24$ lattices using $\epsilon=1$. The effective masses are given in Tables III. Figure 3 shows the effective string tension as a function of time in the two cases. In the absence of a source the approach to the asymptotic value is from above as expected. In the presence of a cold wall, the effective string tension quickly drops below the asymptotic result and then shows a small rise. The signal for the 0^{++} glueball shown in Fig. 4 appears to have a similar trend. These graphs show clearly both the advantages

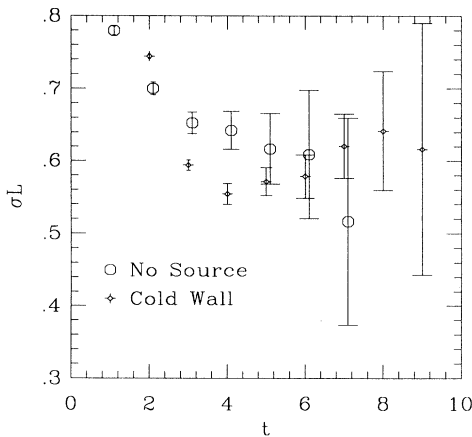


FIG. 3. Comparison of σL results with and without a cold wall source on $12^3 \times 24$ lattices. The data is for $b=2$ smearing, $\epsilon=1.0$ and $N_s=2$.

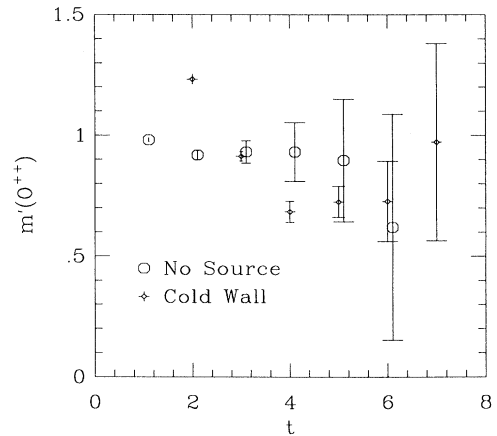


FIG. 4. Comparison of $m'_{0^{++}}$ results with and without a cold wall source on $12^3 \times 24$ lattices. The data is for $b=2$ smearing, $\epsilon=1.0$, $N_s=2$ and 1×1 loop.

and disadvantages of wall sources. The errors at given fixed t are smaller (this is particularly striking considering that the wall source calculation uses three times fewer lattices—see Table I), but the non-uniform convergence can give rise to misleading interpretations. This undesirable behavior negates the advantages of a cold wall source.

VI. COMPARISON OF $b = 1$ AND $b = 2$ SMEARING

We can use the high-statistics runs on $12^3 \times 24$ lattices to compare the $b = 1$ and $b = 2$ smearing methods with $\epsilon = 1$. The results are given in Tables III and IV. Note that the two runs have similar statistics, so that in assessing differences one can directly compare the statistical errors. We note the following.

(a) There is good agreement at all time separations between the $b = 2$ string tension data for $N_s = 2$ and the $b = 1$ data on level $N_s = 4$. These correspond to fat Polyakov lines of similar thickness. As discussed above, for small t the $b = 1$ data shows further convergence with increasing N_s . We cannot check this with the $b = 2$ method since $N_s = 2$ is the highest smearing level on a $12^3 \times 24$ lattice.

(b) The $b = 2$ smearing results for m_{0++} ($N_s = 2$ and 1×2 loops) agree very well with the $b = 1$ results for

loops of similar size and thickness ($N_s \geq 4$ and loop size $\geq 3 \times 3$). In both cases the results appear to have reached their asymptotic values.

(c) Within larger errors, the results for m_{2++} from the two smearing methods agree for loops of similar size and thickness. In this case, however, the numbers do not appear to be asymptotic.

(d) For the same time separations, the statistical errors on loops of similar size and thickness are comparable.

Clearly there is little difference between the two smearing methods. This means that the precise way one builds up the fat loops is not important. The advantage of $b = 2$ smearing is that it takes less computer time to build up a loop of given size and thicknesses: one requires fewer smearing steps and the measured loops are smaller (in blocked lattice units). In the present comparison the computation time per measurement for $b = 1$ smearing was about 1.5 times that for $b = 2$. On the other hand, with a larger number of lattice points, $b = 1$ smearing allows greater flexibility in constructing loops of different size and shape. Since the $b = 2$ method requires less computer time and memory, the optimal combination may be a hybrid of the two methods,¹⁵ with a few $b = 2$ smearing steps followed by some $b = 1$ smearing steps after which loop correlations are measured.

TABLE IV. (a) The σL data for $b = 1$ smearing with $\epsilon = 1.0$ on $12^3 \times 24$ lattices as a function of time separation and smearing level. The statistics is shown as (numbers of bins) \times (configurations per bin). (b) The data for m_{0++} for the same runs as in (a). (c) The data for m_{2++} for the same runs as in (a).

(a)						
$b = 1$ smearing: σL on $12^3 \times 24$ lattices						
t	$N_s = 0$ 23 \times 500	$N_s = 2$ 23 \times 500	$N_s = 3$ 43 \times 500	$N_s = 4$ 43 \times 500	$N_s = 5$ 20 \times 500	$N_s = 6$ 20 \times 500
0-1	3.752(63)	0.999(06)	0.861(03)	0.783(03)	0.730 (04)	0.696(04)
1-2	1.022(53)	0.780(09)	0.734(06)	0.706(06)	0.680(07)	0.665(07)
2-3	0.661(54)	0.671(17)	0.668(11)	0.657(10)	0.657(13)	0.649(12)
3-4		0.627(34)	0.617(21)	0.616(19)	0.605(25)	0.601(24)
4-5		0.626(64)	0.584(36)	0.584(32)	0.570(45)	0.570(43)
(b)						
$b = 1$ smearing: m_{0++} on $12^3 \times 24$ lattices						
t	$N_s = 0$ 23 \times 500	$N_s = 2$ 23 \times 500	$N_s = 3$ 43 \times 500	$N_s = 4$ 43 \times 500	$N_s = 5$ 20 \times 500	$N_s = 6$ 20 \times 500
m_{0++} using 2×2 loops						
0-1	2.32(02)	1.35(01)	1.20(00)	1.09(00)	1.03(01)	0.98(01)
1-2	1.54(08)	1.18(02)	1.08(02)	1.01(01)	0.95(02)	0.91(02)
2-3	1.59(50)	0.98(08)	0.95(04)	0.92(04)	0.95(05)	0.93(05)
3-4		0.78(13)	0.92(09)	0.89(08)	0.96(13)	0.93(12)
4-5		0.75(31)	0.96(25)	0.90(19)	1.03(38)	0.90(27)
m_{0++} using 3×3 loops						
0-1	2.35(02)	1.19(01)	1.09(00)	1.02(00)	0.99(01)	1.06(01)
1-2	1.30(06)	1.08(02)	1.01(01)	0.96(01)	0.91(02)	0.88(02)
2-3	1.71(34)	0.90(06)	0.90(04)	0.88(03)	0.91(05)	0.89(05)
3-4	0.96(97)	0.79(10)	0.90(07)	0.88(07)	0.92(10)	0.90(10)
4-5		0.82(21)	0.91(18)	0.87(14)	0.92(24)	0.81(17)

TABLE IV. (Continued).

(b)						
$b=1$ smearing: $m_{0^{++}}$ on $12^3 \times 24$ lattices						
t	$N_s=0$ 23×500	$N_s=2$ 23×500	$N_s=3$ 43×500	$N_s=4$ 43×500	$N_s=5$ 20×500	$N_s=6$ 20×500
$m_{0^{++}}$ using 4×4 loops						
0-1	3.27(04)	1.09(01)	1.00(00)	0.94(00)	0.90(01)	0.87(01)
1-2	1.00(12)	0.99(02)	0.94(01)	0.91(01)	0.88(02)	0.86(02)
2-3	0.92(33)	0.82(05)	0.85(03)	0.85(03)	0.87(04)	0.86(04)
3-4	0.26(42)	0.82(09)	0.88(06)	0.87(06)	0.89(09)	0.87(08)
4-5		0.72(16)	0.84(13)	0.83(11)	0.89(19)	0.83(16)
$m_{0^{++}}$ using 5×5 loops						
0-1			0.99(01)	0.92(01)	0.88(01)	0.85(01)
1-2			0.91(02)	0.88(02)	0.86(02)	0.85(02)
2-3			0.87(05)	0.86(05)	0.86(05)	0.85(05)
3-4			0.92(09)	0.90(08)	0.88(08)	0.87(08)
4-5			1.07(25)	0.98(20)	0.91(17)	0.86(15)
$m_{0^{++}}$ using 6×6 loops						
0-1			1.12(01)	1.00(01)	0.93(01)	0.88(01)
1-2			0.93(03)	0.89(02)	0.86(02)	0.85(02)
2-3			0.87(06)	0.85(05)	0.84(05)	0.83(05)
3-4			0.91(09)	0.90(08)	0.88(07)	0.88(07)
4-5			1.20(28)	1.04(19)	0.95(16)	0.89(14)
(c)						
$b=1$ smearing: $m_{2^{++}}$ on $12^3 \times 24$ lattices						
t	$N_s=0$ 23×500	$N_s=2$ 23×500	$N_s=3$ 43×500	$N_s=4$ 43×500	$N_s=5$ 20×500	$N_s=6$ 20×500
$m_{2^{++}}$ using 2×2 loops						
0-1	2.89(02)	1.81(01)	1.64(01)	1.53(01)	1.46(01)	1.42(01)
1-2	2.10(17)	1.66(04)	1.54(02)	1.46(02)	1.40(02)	1.35(02)
2-3		1.44(19)	1.51(11)	1.44(08)	1.40(09)	1.33(08)
3-4				1.64(49)	1.13(35)	1.06(28)
$m_{2^{++}}$ using 3×3 loops						
0-1	3.00(03)	1.61(01)	1.50(01)	1.44(01)	1.42(01)	1.52(01)
1-2	1.95(22)	1.53(03)	1.45(02)	1.39(02)	1.34(02)	1.29(02)
2-3	1.61(97)	1.37(15)	1.40(08)	1.34(07)	1.31(07)	1.28(07)
3-4			1.54(42)	1.38(30)	1.07(26)	1.00(24)
$m_{2^{++}}$ using 4×4 loops						
0-1	3.91(05)	1.48(01)	1.38(00)	1.32(00)	1.28(01)	1.26(01)
1-2	2.06(43)	1.41(02)	1.36(01)	1.32(01)	1.29(02)	1.26(02)
2-3		1.23(09)	1.25(06)	1.23(05)	1.21(06)	1.19(06)
3-4		1.74(66)	1.27(23)	1.20(18)	1.04(19)	1.02(17)
$m_{2^{++}}$ using 5×5 loops						
0-1			1.35(01)	1.28(01)	1.24(01)	1.21(01)
1-2			1.27(02)	1.24(02)	1.22(02)	1.21(02)
2-3			1.16(07)	1.15(06)	1.14(06)	1.14(06)
3-4			0.96(17)	1.00(16)	1.02(15)	1.03(16)
$m_{2^{++}}$ using 6×6 loops						
0-1			1.47(01)	1.34(01)	1.27(01)	1.23(01)
1-2			1.25(02)	1.22(02)	1.20(02)	1.19(02)
2-3			1.09(07)	1.11(06)	1.11(06)	1.11(06)
3-4			1.12(26)	1.10(21)	1.09(18)	1.09(17)

VII. RESULTS

In addition to the runs on $12^3 \times 24$ lattices just described, we have long runs on $9^3 \times 24$ and $15^3 \times 24$ lattices using $b=1$ smearing and $\epsilon=1$. The results from the largest lattice are given in Tables V.

It is interesting to observe how the dependence of the signal on N_s varies with time separation. The effective

mass should tend to the same asymptotic value for all N_s , as contributions from higher states die away. Nevertheless, the errors should be larger for small N_s because these operators couple more strongly to ultraviolet fluctuations. These expectations are borne out by our results. For example, Table V(a) shows that by $t=4/5$ the results from all our values for N_s agree, but the error increases

TABLE V. (a) The σL data for $b=1$ smearing with $\epsilon=1.0$ on $15^3 \times 24$ lattices as a function of time separation and smearing level. (b) The data for m_{0++} for the same runs as in (a). (c) The data for m_{2++} for the same runs as in (a).

(a)				
$b=1$ smearing: σL on $15^3 \times 24$ lattices				
t	$N_s=3$ 30×500	$N_s=4$ 30×500	$N_s=5$ 30×500	$N_s=6$ 30×500
0-1	1.2333(004)	1.109(004)	1.029(004)	0.975(004)
1-2	1.016(011)	0.971(010)	0.939(009)	0.913(008)
2-3	0.894(027)	0.884(023)	0.873(021)	0.863(020)
3-4	0.762(068)	0.759(057)	0.759(051)	0.761(047)
4-5	0.623(106)	0.659(087)	0.674(080)	0.678(077)
(b)				
$b=1$ smearing: m_{0++} on $15^3 \times 24$ lattices				
t	$N_s=3$ 30×500	$N_s=4$ 30×500	$N_s=5$ 30×500	$N_s=6$ 30×500
m_{0++} using 2×2 loops				
0-1	1.21(01)	1.10(01)	1.03(00)	0.99(00)
1-2	1.08(02)	1.01(01)	0.97(01)	0.93(01)
2-3	0.88(04)	0.86(03)	0.85(03)	0.84(03)
3-4	0.78(08)	0.78(07)	0.78(07)	0.78(06)
4-5	0.89(19)	0.83(15)	0.80(14)	0.78(12)
m_{0++} using 3×3 loops				
0-1	1.10(01)	1.03(00)	1.00(00)	1.05(01)
1-2	1.01(01)	0.96(01)	0.92(01)	0.89(01)
2-3	0.86(03)	0.85(03)	0.84(03)	0.83(03)
3-4	0.76(07)	0.76(06)	0.76(06)	0.75(06)
4-5	0.82(15)	0.80(13)	0.78(12)	0.77(12)
m_{0++} using 4×4 loops				
0-1	1.01(00)	0.95(00)	0.91(00)	0.88(00)
1-2	0.95(01)	0.92(01)	0.89(01)	0.87(01)
2-3	0.83(03)	0.82(03)	0.82(02)	0.81(02)
3-4	0.75(06)	0.75(05)	0.75(05)	0.75(05)
4-5	0.75(12)	0.74(11)	0.74(10)	0.74(10)
m_{0++} using 5×5 loops				
0-1	1.00(01)	0.93(01)	0.89(01)	0.86(01)
1-2	0.91(01)	0.89(01)	0.87(01)	0.85(01)
2-3	0.81(03)	0.80(02)	0.80(02)	0.80(02)
3-4	0.72(06)	0.72(05)	0.72(05)	0.72(05)
4-5	0.69(10)	0.71(09)	0.72(09)	0.72(09)
m_{0++} using 6×6 loops				
0-1	1.14(01)	1.01(01)	0.94(01)	0.90(01)
1-2	0.94(01)	0.90(01)	0.88(01)	0.86(01)
2-3	0.82(03)	0.81(03)	0.80(03)	0.80(02)
3-4	0.69(06)	0.69(05)	0.70(05)	0.70(05)
4-5	0.68(11)	0.69(10)	0.71(09)	0.72(09)

TABLE V. (Continued).

t	(c) $m_{2^{++}}$ on $15^3 \times 24$ lattices			
	$N_s=3$ 30×500	$N_s=4$ 30×500	$N_s=5$ 30×500	$N_s=6$ 30×500
$b=1$ smearing: $m_{2^{++}}$ using 2×2 loops				
0-1	1.64(01)	1.53(01)	1.46(01)	1.43(01)
1-2	1.53(04)	1.45(03)	1.40(03)	1.36(03)
2-3	1.37(13)	1.30(10)	1.26(08)	1.22(07)
3-4	1.34(40)	1.27(27)	1.27(24)	1.24(22)
$m_{2^{++}}$ using 3×3 loops				
0-1	1.50(01)	1.44(01)	1.42(01)	1.52(01)
1-2	1.44(03)	1.39(03)	1.35(03)	1.32(03)
2-3	1.33(10)	1.29(08)	1.26(07)	1.25(08)
3-4	1.30(28)	1.23(22)	1.16(21)	1.07(22)
$m_{2^{++}}$ using 4×4 loops				
0-1	1.38(01)	1.32(01)	1.28(01)	1.26(01)
1-2	1.36(03)	1.33(02)	1.30(02)	1.28(02)
2-3	1.26(06)	1.22(06)	1.20(05)	1.19(05)
3-4	1.30(21)	1.27(19)	1.25(19)	1.23(19)
$m_{2^{++}}$ using 5×5 loops				
0-1	1.35(01)	1.28(01)	1.24(00)	1.22(00)
1-2	1.31(02)	1.28(02)	1.25(02)	1.24(02)
2-3	1.20(05)	1.19(05)	1.18(05)	1.18(05)
3-4	1.15(17)	1.16(16)	1.17(16)	1.17(17)
$m_{2^{++}}$ using 6×6 loops				
0-1	1.47(01)	1.34(01)	1.27(00)	1.23(00)
1-2	1.32(02)	1.28(02)	1.25(02)	1.23(02)
2-3	1.21(06)	1.20(05)	1.19(05)	1.18(04)
3-4	0.97(18)	1.03(15)	1.08(14)	1.12(14)

as N_s decreases. Thus large values of N_s are preferred both because the asymptotic mass is approached more quickly, and because the errors are smaller. Similar results are expected for the loop size dependence of glueball signals: smaller loops should yield effective masses with larger errors even when they have reached their asymptotic value. This is indeed the pattern we see.

We expect the absolute errors in the correlation functions to be independent of t for large t , while the signal drops exponentially. Thus the errors in m_{eff} should grow as $\exp(mt)$, where m is the asymptotic mass in the channel. Our errors are consistent with this expectation.

As discussed above, large loops have the greatest overlap with scalar and tensor glueballs. The optimization analysis at $t=0/1$ found very little difference between 4×4 , 5×5 , and 6×6 loops, though 5×5 loops were slightly favored. From Tables V(b) and V(c) [and also IV(b) and IV(c)], we see that there is no significant difference between these three loop sizes at longer times. For $b=2$ smearing, however, Tables III(b) and III(c) show that, for $N_s=2$, the signals from 2×2 loops are much poorer than those from 1×2 loops. Thus the fattened 8×8 loop has a smaller overlap with the glueball than fattened loops of size 4-6, suggesting that the glue-

balls have a size of $\sim 5a$. Using $\sqrt{\sigma}=420$ MeV to set the lattice scale, we get $1/a \approx 2$ GeV and $5a \approx 0.5$ fm. This rough measure of glueball size finds them to be comparable in extent to other hadrons.

The lack of signal in 1×1 loop (see Tables IV and V) suggests that the wave function is small at the origin. A possible shape for the 0^{++} glueball consistent with this behavior is a spherically symmetrized doughnut of chromoelectric flux.

The best estimates for masses from all our long runs are collected in Table VI. Since in many cases the signal does not persist long enough to demonstrate convergence to the asymptotic value, we quote results for the two longest time separations having statistically significant data.

The results for σ on the smallest lattice are significantly less than those on the $12^3 \times 24$ lattices, although consistent within errors with the results from the largest lattices. The finite-size scaling form suggested by integration of string fluctuations is¹⁶

$$\sigma_L = \sigma_\infty - \frac{\pi}{3L^2} + O(L^{-3}), \quad (7.1)$$

where $\sqrt{\sigma_\infty}$ is the infinite-volume result. The resulting

TABLE VI. Our best estimates for $\sqrt{\sigma}$, $m_{0^{++}}$ and $m_{2^{++}}$ from the various data samples. We give time separation t , smearing level N_s , and loop size S_L from which these numbers have been extracted.

	t	Best estimates			
		$9^3 \times 24$ $b=1(\epsilon=1.0)$	$12^3 \times 24$ $b=2(\epsilon=1.0)$	$12^3 \times 24$ $b=1(\epsilon=1.0)$	$15^3 \times 24$ $b=1(\epsilon=1.0)$
$\sqrt{\sigma}$	3-4	0.206(3)	0.231(4)	0.224(4)	0.225(7)
	4-5	0.204(4)	0.228(8)	0.218(7)	0.212(12)
		$N_s=6$	$N_s=2$	$N_s=5,6$	$N_s=4,5,6$
$\sqrt{\sigma_\infty}$	4-5	0.234(4)	0.243(8)	0.234(7)	0.223(12)
$m_{0^{++}}$	2-3	0.76(2)	0.90(4)	0.86(4)	0.81(2)
	3-4	0.74(5)	0.88(11)	0.88(8)	0.74(5)
		$N_s=6$ $S_L=3,4$	$N_s=2$ $S_L=1 \times 2$	$N_s=4,5,6$ $S_L=4,5,6$	$N_s=4,5,6$ $S_L=4,5$
$m_{2^{++}}$	2-3	1.20(7)	1.20(5)	1.13(6)	1.19(5)
	3-4	1.11(19)	1.22(15)	1.06(17)	1.20(18)
		$N_s=6$ $S_L=4$	$N_s=2$ $S_L=1 \times 2$	$N_s=5,6$ $S_L=5,6$	$N_s=5,6$ $S_L=4,5$

values of $\sqrt{\sigma_\infty}$ are shown in the table. The shifts bring the three volumes into reasonable agreement.

The scalar glueball mass shows a perplexing finite-volume dependence, the mass first increasing and then decreasing as the volume gets larger. This is in contrast with results at $K_F=6.0$ on the Wilson axis, which has a similar lattice spacing to our lattices. Michael and Teper⁸ find that σ and $m_{0^{++}}$ are almost unchanged as the lattice size increases from 10 to 20. We do not have enough data to check whether the difference is due to statistical errors and incomplete convergence, or whether there is a significant difference between the two lattice actions. Michael and Teper also find that $m_{2^{++}}$ increases by $\sim 20\%$ from 10^3 to 16^3 lattices, while our data for $m_{2^{++}}$ is consistent with no finite volume dependence.

Another factor clouding the issue is that, for small lattices, the glueball signal may be contaminated by a torelon-antitorelon pair. This can happen if $2\sigma L$ is less than the glueball mass, as pointed out by Michael.¹⁷ In our data this crossover occurs at $L \approx 9$ for the 0^{++} glueball, and at $L \approx 12$ for the 2^{++} glueball. Given this, we simply use the results from the $15^3 \times 24$ lattices as our best estimates:

$$\begin{aligned} m_{0^{++}}/\sqrt{\sigma} &= 3.5(3) , \\ m_{2^{++}}/m_{0^{++}} &= 1.6(2) . \end{aligned} \quad (7.2)$$

These results are consistent with those obtained with the Wilson action.⁸ It is encouraging that the results are, within 10–15% errors, independent of the lattice action at scale $1/a=2$ GeV. The main caveat is that all masses are of order 1 in lattice units. The only way to check scaling is to work at weaker coupling.

VIII. CONCLUSIONS

We have introduced and tested a variant of previous smearing methods. We find that $b=1$ smearing can be

competitive with only moderate numbers of smearing steps ($N_s \approx 5$), as long as one uses large values of the smearing parameter ($\epsilon \approx 1$) and uses large loops as the starting template. The use of small value of N_s is important in order to reduce computer usage.

We find that fat 5×5 loops give the best signal for both 0^{++} and 2^{++} states at a lattice scale of $1/a \approx 2$ GeV. This implies that the glueballs are of typical hadronic size, ≈ 0.5 fm.

We find that the results obtained using the cold wall source show a non-uniform convergence as a function of the time separation. Consequently, if the signal does not extend far enough, one cannot extract reliable answers.

The iterative smearing procedures discussed here are easy to implement, but do not give detailed information about the glueball wave function. A better approach may be to construct an elaborate smearing procedure that maps onto the wave function in one step (i.e., including many more paths of longer length in the smearing step than those shown in Figs. 1 and 2).

Finally we note that it will be difficult to improve mass estimates using the variational method, since for time separation $2/3$ and larger the glueball results are insensitive to loop size for loops bigger than 2×2 . Thus, even if we tune the variational operator using time separation $0/1$, the mass estimate will not improve for time separation greater than $1/2$.

ACKNOWLEDGEMENTS

This work was supported in part by NSF Grant No. PHY89-04035, supplemented by funds from the National Aeronautics and Space Administration. S.R.S. was supported in part by the DOE Office of Junior Investigator Program through Contract No. DE-AT06-88ER40423 and the Alfred P. Sloan Foundation. The $b=1$, $12^3 \times 24$ calculations were done on the JPL/Caltech Cray. We are very grateful to the staff at JPL for their support and interest in the calculation during the shakedown period. In particular we would like to thank G. C. Fox and P. Mes-

sina for their encouragement. The $b=2$, $12^3 \times 24$ calculations were carried out on the CERN Cray, and we thank the DD division for their assistance. We are grateful to A. White and the Advanced Computing Laborato-

ry at Los Alamos for calculation on $9^3 \times 24$ lattices. Finally, we express our gratitude to R. Roskies for allocation of time at the Pittsburgh Supercomputing Center, where the $15^3 \times 24$ runs were done.

-
- ¹For a recent review, see C. Michael, in *Lattice '89*, proceedings of the International Symposium, Capri, Italy, 1989, edited by R. Petronzio *et al.* [Nucl. Phys. B (Proc. Suppl.) **17**, 59 (1990)].
- ²F. Brandstaeter, A. Kronfeld, and G. Schierholz, Nucl. Phys. **B345**, 709 (1990).
- ³For a recent review, see T. Burnett and S. Sharpe, Annu. Rev. Nucl. Part. Sci. **40**, 327 (1990).
- ⁴M. Teper, Phys. Lett. B **183**, 345 (1987).
- ⁵T. DeGrand, Phys. Rev. D **36**, 176 (1987); **36**, 3522 (1987).
- ⁶APE Collaboration, M. Albanese *et al.*, Phys. Lett. B **192**, 163 (1987).
- ⁷APE Collaboration, P. Bacilieri *et al.*, Phys. Lett. B **205**, 535 (1988).
- ⁸C. Michael and M. Teper, Nucl. Phys. **B314**, 347 (1989).
- ⁹R. Gupta, G. Guralnik, A. Patel, T. Warnock, and C. Zemach, Phys. Lett. **161B**, 352 (1985).
- ¹⁰A. Patel, R. Gupta, G. Guralnik, G. Kilcup, and S. Sharpe, Phys. Rev. Lett. **57**, 1288 (1986).
- ¹¹R. Gupta, G. Kilcup, A. Patel, S. Sharpe, and Ph. de Forcrand, Mod. Phys. Lett. A **3**, 1367 (1988).
- ¹²J. Mandula, G. Zweig, and J. Govaerts, Nucl. Phys. **B228**, 91 (1983).
- ¹³R. Swendsen, Phys. Rev. Lett. **47**, 1775 (1981).
- ¹⁴APE Collaboration, M. Albanese *et al.*, Phys. Lett. B **197**, 400 (1987); L. Fernandez and E. Marinari, Nucl. Phys. **B295**, 51 (1988).
- ¹⁵APE Collaboration, P. Bacilieri *et al.*, Nucl. Phys. **B318**, 553 (1989).
- ¹⁶M. Lüscher, Nucl. Phys. **B180** [FS2], 317 (1981); R. Pisarski and O. Alvarez, Phys. Rev. D **26**, 3735 (1982).
- ¹⁷C. Michael, J. Phys. G **13**, 1001 (1987).